JOURNAL
OF
THE ROYAL
SOCIETY
Interface

Caecilian jaw-closing mechanics: integrating two muscle systems

Thomas Kleinteich, Alexander Haas and Adam P Summers

References	**This article cites 41 articles, 6 of which can be accessed free** http://rsif.royalsocietypublishing.org/content/5/29/1491.full.html#ref-list-1
Subject collections	Articles on similar topics can be found in the following collections biophysics (70 articles)
Email alerting service	Receive free email alerts when new articles cite this article - sign up in the box at the top right-hand corner of the article or click **here**

To subscribe to *J. R. Soc. Interface* go to: **http://rsif.royalsocietypublishing.org/subscriptions**

Caecilian jaw-closing mechanics: integrating two muscle systems

Thomas Kleinteich[1,*], **Alexander Haas**[1] **and Adam P. Summers**[2]

[1]*Universität Hamburg, Biozentrum Grindel und Zoologisches Museum, Martin-Luther-King-Platz 3, 20146 Hamburg, Germany*
[2]*University of California Irvine, 321 Steinhaus, Irvine, CA 92697, USA*

Caecilians (Lissamphibia: Gymnophiona) are unique among vertebrates in having two sets of jaw-closing muscles, one on either side of the jaw joint. Using data from high-resolution X-ray radiation computed tomography scans, we modelled the effect of these two muscle groups (*mm. levatores mandibulae* and *m. interhyoideus posterior*) on bite force over a range of gape angles, employing a simplified lever arm mechanism that takes into account muscle cross-sectional area and fibre angle. Measurements of lever arm lengths, muscle fibre orientations and physiological cross-sectional area of cranial muscles were available from three caecilian species: *Ichthyophis* cf. *kohtaoensis*; *Siphonops annulatus*; and *Typhlonectes natans*. The maximal gape of caecilians is restricted by a critical gape angle above which the *mm. levatores mandibulae* will open the jaw and destabilize the mandibular joint. The presence of destabilizing forces in the caecilian jaw mechanism may be compensated for by a mandibular joint in that the fossa is wrapped around the condyle to resist dislocation. The caecilian skull is streptostylic; the quadrate–squamosal complex moves with respect to the rest of the skull. This increases the leverage of the jaw-closing muscles. We also demonstrate that the unusual jaw joint requires streptostyly because there is a dorsolateral movement of the quadrate–squamosal complex when the jaw closes. The combination of the two jaw-closing systems results in high bite forces over a wide range of gape angles, an important advantage for generalist feeders such as caecilians. The relative sizes and leverage mechanics of the two closing systems allow one to exert more force when the other has a poor mechanical advantage. This effect is seen in all three species we examined. In the aquatic *T. natans*, with its less well-roofed skull, there is a larger contribution of the *mm. levatores mandibulae* to total bite force than in the terrestrial *I.* cf. *kohtaoensis* and *S. annulatus*.

Keywords: Gymnophiona; amphibian cranial morphology; bite force modelling; high resolution μCT; automated measurement of muscle fibre angles

1. INTRODUCTION

Caecilians (Gymnophiona) are fossorial limbless amphibians, comprising 171 species with circumtropical distribution (Frost 2007). Their burrowing lifestyle places special demands on their cranial anatomy, and the caecilian skull is compact and wedge shaped, with many bones fused into compound elements (for a review see Wake 2003). Caecilians are also unique among vertebrates in possessing two sets of jaw-closing mechanisms that act on either side of the jaw joint. In addition to the usual complement of jaw adductors anterior to the jaw joint (*mm. levatores mandibulae*), a hyobranchial muscle posterior to the joint (*m. interhyoideus posterior* (IHP)) acts as an accessory jaw-closing muscle.

The jaw-closing function of the IHP was proposed by Bemis *et al.* (1983) and Nussbaum (1983) who realized

that its insertions on the ventral side of the retro-articular process of the lower jaw allowed it to adduct the mandible (figure 1). Using electromyography, Bemis *et al.* (1983) showed that the IHP acts synergistically with the primary jaw-closing muscles. The jaw-closing function of the IHP has been proposed as an adaptation to a fossorial lifestyle (Nussbaum 1983). The reasoning is that in compact caecilian skulls, space for the *mm. levatores mandibulae* is restricted by the squamosal, a bone that covers large parts of the lateral face of the skull. The restriction on the size of the *mm. levatores mandibulae* demands the use of the IHP as an accessory jaw-closing muscle to generate appropriate bite forces.

Although the cranium in caecilians is compact and solid, the morphology of the quadrate and the squamosal (quadrate–squamosal complex) led to the hypothesis that caecilian skulls are kinetic (streptostylic; Luther 1914; Marcus *et al.* 1933; De Villiers 1936; Iordanski 1990, 2000; Wilkinson & Nussbaum 1997). Indeed, manipulating the skull of a freshly killed
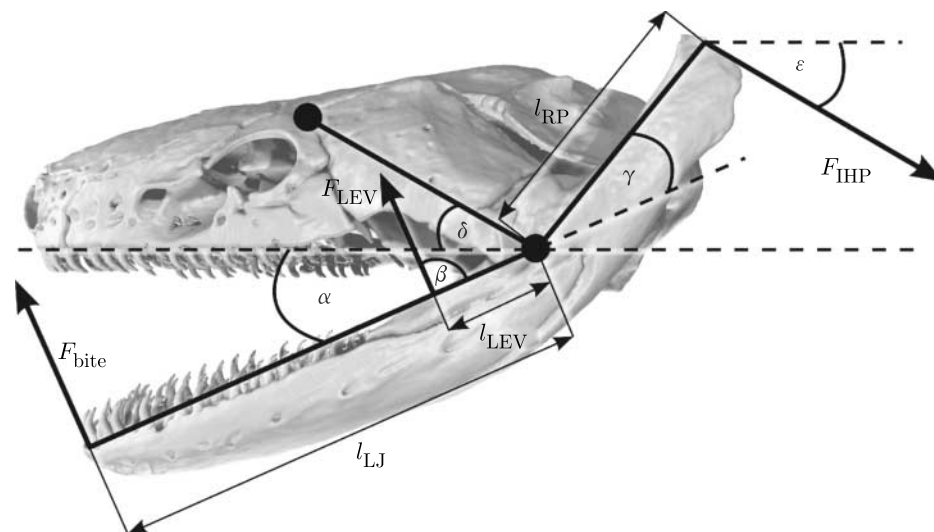
Figure 1. Representation of the lever arm model used to predict bite forces in the caecilian jaw-closing mechanism drawn over a reconstruction of the skull in lateral view of *I.* cf. *kohtaoensis*. Bite forces were calculated for a range of gape angles (α) from 0° to 90°. Two jaw-closing mechanisms, one actuated by the *mm. levatores mandibulae* and the other actuated by the IHP, are shown. The bite force at the tip of the lower jaw F_{bite} is a function of the forces generated by the two closing systems. The *mm. levatores mandibulae* closure system is described by the force generated by the muscles (F_{LEV}), acting on an input lever arm l_{LEV}, with a muscle fibre orientation of β. The IHP closure system acts on a lever arm l_{RP}, with a force of F_{IHP} and a fibre orientation of ε. Two aspects of skull anatomy are captured with angular measurements: the angle of the quadrate–squamosal complex (δ) and the angle of the retroarticular process of the lower jaw with a line drawn from the lower jaw joint to the tip of the lower jaw (γ).

Dermophis mexicanus specimen showed that the quadrate and the squamosal could rotate slightly (Wake & Hanken 1982). A model of bite force generated by the IHP demonstrated the unusual and counter-intuitive result that force steadily decreases during jaw closure. However, two factors can ameliorate this loss in force: a retroarticular process that curves upward, giving a better mechanical advantage (O'Reilly 2000) and the streptostylic joints in the skull, which act as a second leverage system (Summers & Wake 2005).

Previous mathematical descriptions of the function of the IHP were based on the assumption that muscle fibre orientation in the IHP is aligned exactly along the long axis of the animal and the force acts in caudal direction (Summers & Wake 2005). However, the studies of the cranial musculature in caecilians (Wiedersheim 1879; Luther 1914; Lawson 1965; Bemis *et al.* 1983; Nussbaum 1983; Iordanski 1996; Wilkinson & Nussbaum 1997; Kleinteich & Haas 2007) show that the fibre orientation of the IHP in most caecilian species is oblique rather than purely anteroposterior; the muscle fibres run in the caudal *and* ventral directions. A second simplification in the previous model was to ignore the jaw-closing function of the *mm. levatores mandibulae*. These are the only jaw-closing muscles in most other vertebrates and are quite substantial in size, so it is important that any model of caecilian jaw function includes the contribution of these muscles.

The goals of this study are fivefold: (i) we propose a new model of jaw function that includes the contribution of fibre angles that are not aligned with the long axis of the body, (ii) we extend the model to include the ancestral jaw-closing muscles, the *mm. levatores mandibulae*, (iii) we estimate the effective mechanical advantages (EMAs) of these two jaw-closing systems over different gape angles to test the hypothesis that the two systems contribute best to different parts of jaw closure, (iv) with values derived from high-resolution, synchrotron-based X-ray radiation computed tomography (CT) scan data, we calculate a theoretical bite force across a range of gapes and the contributions of the two closing systems to the maximal bite force, and (v) we use physical and computer models to describe the complex movements at the jaw joint during the doubly actuated closure of the gape.

2. MATERIAL AND METHODS

We studied the jaw lever mechanics of three specimens from different caecilian species (table 1; figure 2): *Ichthyophis kohtaoensis* Taylor, 1960; *Typhlonectes natans* (Fischer *in* Peters, 1880); and *Siphonops annulatus* (Mikan, 1820). All the specimens are stored in the herpetological collection of the zoological museum, Hamburg (ZMH). Our sampling comprises basal (*Ichthyophis* cf. *kohtaoensis*) and derived clades within the Gymnophiona (figure 2) and two different skull architectures: *I.* cf. *kohtaoensis* and *S. annulatus* have stegokrotaphic skulls (closed temporal region; figure 2), and *T. natans* has a zygokrotaphic skull (temporal region with wide gap between squamosal and parietal; figure 2). Owing to unsolved problems in the taxonomy of and within the genus *Ichthyophis* (see Gower *et al.* 2002), we use *I.* cf. *kohtaoensis* herein for specimen ZMH A08981. The current taxonomic status of *I. kohtaoensis* is highly debated and under revision. Further, the genus *Ichthyophis* has been shown to be paraphyletic (Gower *et al.* 2002; Frost *et al.* 2006; Roelants *et al.* 2007; figure 2).

The specimens were decapitated between the fifth and sixth annuli (i.e. in the anterior trunk region). All specimens had been stored in 70% EtOH. We

Table 1. Specimens used in this study.

| ID	species name	TL (mm)	sample length (before drying) (mm)	sample length (after drying) (mm)	sample diameter (mm)	skull length (mm)	skull width (mm)	locality
ZMH A08981	*Ichthyophis* cf. *kohtaoensis*	265	24	24	9	10.65	7.00	pet trade; unknown locality
ZMH A00235	*Siphonops annulatus*	280	37	36	12	15.73	10.91	Sao Paulo, Brazil
ZMH A08984	*Typhlonectes natans*	330	26	25	9	12.39	7.40	no locality; from Ethological laboratory, Zoological Institute, Hamburg
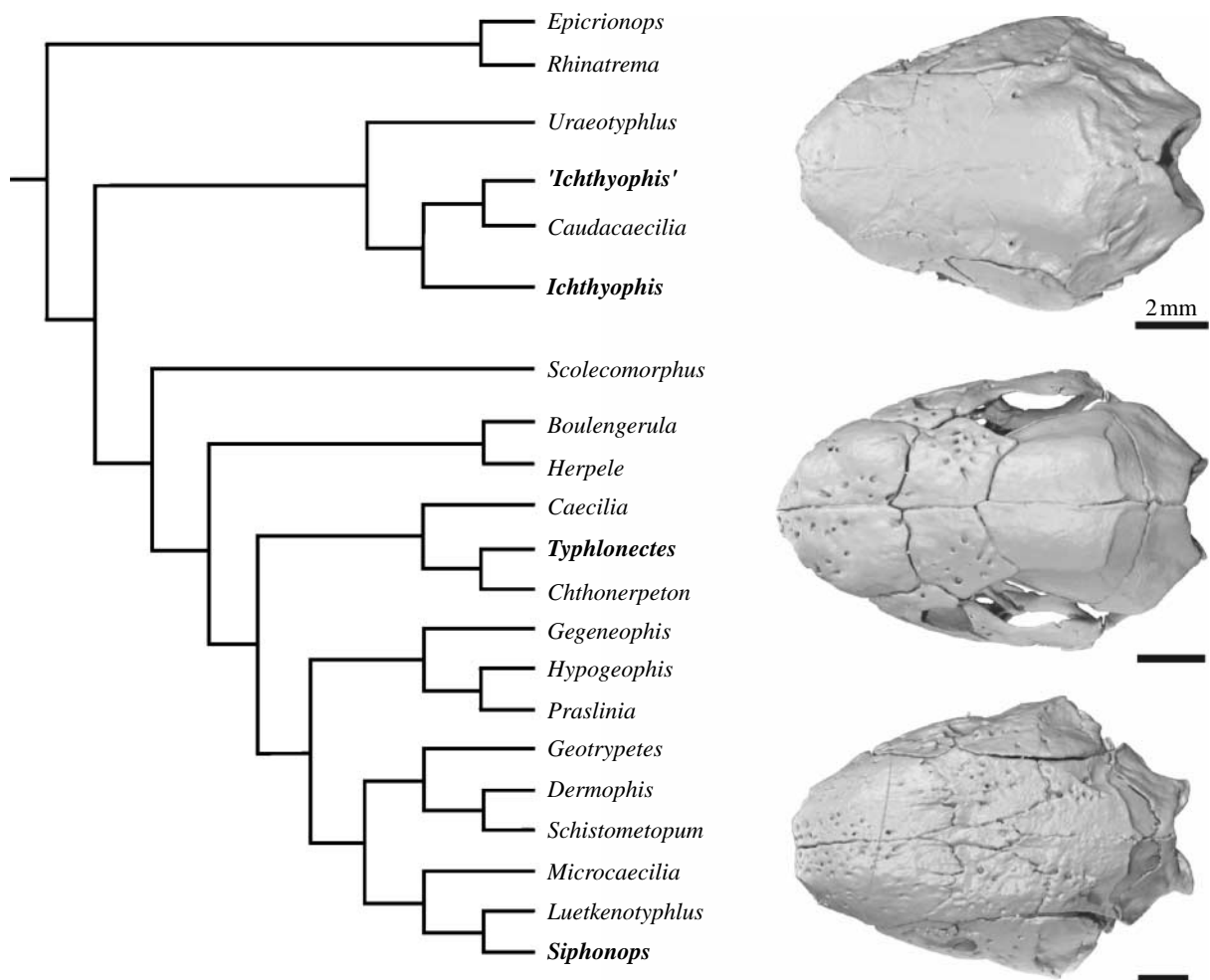
Figure 2. Phylogeny of the Gymnophiona (Roelants *et al.* 2007) showing the genera of the species for which we modelled jaw-closing forces in bold. *Ichthyophis* is a paraphyletic genus that appears in two places on the cladogram and we do not know to which clade *I.* cf. *kohtaoensis* belongs. The skulls are three-dimensional reconstructions from CT image data from *I. kohtaoensis*, *T. natans* and *S. annulatus* shown in dorsal view to emphasize the differences in the temporal region.

stepwise (50 and 30% EtOH, respectively) transferred the separated heads to distilled water; every step was maintained for 24 hours. We freeze dried the specimens following the procedure by Meryman (1960, 1961). The separated heads were frozen at −80°C for 4 hours. After freezing, we dried the samples under low pressure for 4 days. Upon visual inspection, the heads were unchanged after freeze drying; however, there were minor changes in the size of the samples (table 1).

High-resolution, synchrotron-based X-ray CT imaging was performed at Beamline W2 (maintained by the GKSS research centre, Geesthacht) of the DORIS III accelerator ring at the German Electron Synchrotron (DESY) in Hamburg, Germany. The specimens were scanned with a 30 keV X-ray beam. X-ray images were captured over a rotation of 180° in 0.25° steps for the *I.* cf. *kohtaoensis* and *T. natans* specimens, and the *S. annulatus* specimen was rotated 360°. The resulting X-ray dataset was converted to a VGStudio Max

(Volume Graphics GmbH, Heidelberg, Germany) volume rendering dataset. The datasets have a resolution of 6.83 μm (*I.* cf. *kohtaoensis* and *T. natans*) and 9.2 μm (*S. annulatus*) in *x*, *y* and *z* orientations. Neighbouring voxels of the volume dataset have been merged to reduce the size of the dataset (binding). Different graduations of these resampled datasets (twofold, threefold and fourfold bindings) were available for analysis. We used the software packages VGSTUDIO MAX v. 1.2 and AMIRA v. 4.1 (Mercury Computer Systems) for processing, analysing and segmentation of the resulting volumetric three-dimensional datasets. Surface rendering and animation were performed with Alias Wavefront MAYA v. 6.0.

The model used to calculate force transmission of the IHP is based on the model presented by Summers & Wake (2005). To account for fibre orientations of the IHP, we added fibre angle ε to the model (figure 1). We calculated the EMA$_{\text{IHP}}$ (bite force per unit muscle force; based on Biewener 1989) for the IHP by (figure 1)

$$\text{EMA}_{\text{IHP}} = F_{\text{bite}}/F_{\text{IHP}} = \sin(\alpha + \gamma + \varepsilon) \times (l_{\text{RP}}/l_{\text{LJ}}) \\ + \sin(\delta - \varepsilon) \times \cos(\alpha + \delta), \quad (2.1)$$

where F_{bite} is the output bite force; F_{IHP} is the force generated by the IHP; l_{RP} is the length of the retro-articular process of the lower jaw; l_{LJ} is the distance from the rostral tip of the lower jaw to the jaw articulation; α is the gape angle; γ is the retroarticular angle with respect to the anteroposterior axis; δ is the quadrate–squamosal angle with respect to the anteroposterior axis; and ε is the muscle fibre orientation of the IHP with respect to the anteroposterior axis. In this equation and the next, the first term represents the force generated through the conventional simple lever system of the jaws and the second term accounts for the streptostylic suspension of the jaws.

We developed a second lever arm model for the *mm. levatores mandibulae* group (figure 1). This group comprises three muscles in adult caecilians: *m. levator mandibulae articularis*; *m. levator mandibulae internus*; and *m. levator mandibulae longus* (Wiedersheim 1879; Luther 1914; Edgeworth 1935; Lawson 1965; Bemis *et al.* 1983; Iordanski 1996; Wilkinson & Nussbaum 1997; a table of synonyms was presented by Kleinteich & Haas 2007). The EMA for single muscles in this group EMA$_{\text{LEV}}$ is calculated by

$$\text{EMA}_{\text{LEV}} = F_{\text{bite}}/F_{\text{LEV}} \\ = \sin(\beta - \alpha) \times (l_{\text{LEV}}/l_{\text{LJ}}) + \sin(\beta + \delta) \\ \times \cos(\alpha + \delta), \quad (2.2)$$

where F_{bite} is the output bite force; F_{LEV} is the force generated by muscles of the *mm. levatores mandibulae* group; l_{LEV} is the distance from the insertion of the muscles to the jaw articulation; l_{LJ} is the distance from the rostral tip of the lower jaw to the jaw articulation; α is the gape angle; β is the muscle fibre orientation of the muscles with respect to the anteroposterior axis; and δ is the quadrate–squamosal angle with respect to the anteroposterior axis.

Besides the *mm. levatores mandibulae* group, the *nervus trigeminus* innervated jaw musculature of caecilians comprises three additional muscles that are not considered in this paper, i.e. the *m. intermandibularis*,

the *m. levator quadrati* and the *m. pterygoideus* (Iordanski 1996; Haas 2001; Kleinteich & Haas 2007). The *m. interhyoideus* lowers the buccal floor. The function of the *m. levator quadrati* and *m. pterygoideus* is poorly known; however, both insert on the quadrate and thus are likely to be involved in movements of the quadrate (streptostyly) rather than jaw closure.

Measurements of anatomical characters are based on lateral views of rendered CT datasets. We used the freely available image analysis software IMAGEJ v. 1.36b (NIH; http://rsb.info.nih.gov/ij/download.html) for all measurements. We did all measurements for both sides of the body of the animals; the average value of both measurements was used for further calculations.

For measurements of muscle fibre orientations (β and ε), we generated 8 bit grey-scale image stacks of sagittal sections parallel to the muscle in the CT datasets. These image stacks were generated with the *oblique slice function* of AMIRA. For every investigated muscle, we adjusted the plane of section so that sections were parallel to the muscle fibres in lateral view. We converted the grey-scale image stacks into binary data with the *adjust> threshold* function of IMAGEJ. The resulting dataset (figure 3c) contained only muscula-ture (black) and background (white). Muscle fibre orientations were measured automatically with IMAGEJ, and to reduce noise we excluded particles less than 25 pixels in area and with a circularity greater than 0.3 (figure 3d) from the analysis. Measured muscle fibre angles are distributed (figure 3e) around a mean value. Standard deviations of muscle fibre orientations are given in table 2. The standard deviation of muscle fibre angles can be interpreted as an estimate for the diversity of fibre orientations within a muscle. We calculated EMAs for the mean and the minimal and maximal values that were derived from the standard deviation of muscle fibre orientations. However, muscles are treated as idealized parallel-fibred structures herein and the mean fibre orientation was used for interpretation of the jaw-closing mechanism.

Theoretical forces that can be generated by a single muscle were calculated by

$$F_{\text{muscle}} = \left(\frac{V}{l}\right) \times p_{\text{MIS}}, \quad (2.3)$$

where F_{muscle} is the force generated by a muscle; V is the volume of the muscle; l is the length of the muscle in the direction of the fibre orientation; and p_{MIS} is the maximal isometric stress ($p_{\text{MIS}} = 250$ kPa; Herzog 1994). The ratio of muscle volume to muscle length is a measure for physiological cross-sectional area (PCSA).

Total bite force for the entire jaw-closing system (i.e. both jaw-closing systems and both sides of the skull) is calculated as the doubled sum of bite forces from single muscles, assuming bilateral symmetry.

We measured volumes and lengths of the muscles by separating single muscles out of the CT datasets (segmentation). Surfaces were generated out of the segmented datasets and measured with the *lineprobe* and *areavolume* tools in AMIRA. Volume and length measurements are averages of values from both sides of the body. To interactively explore possible movements
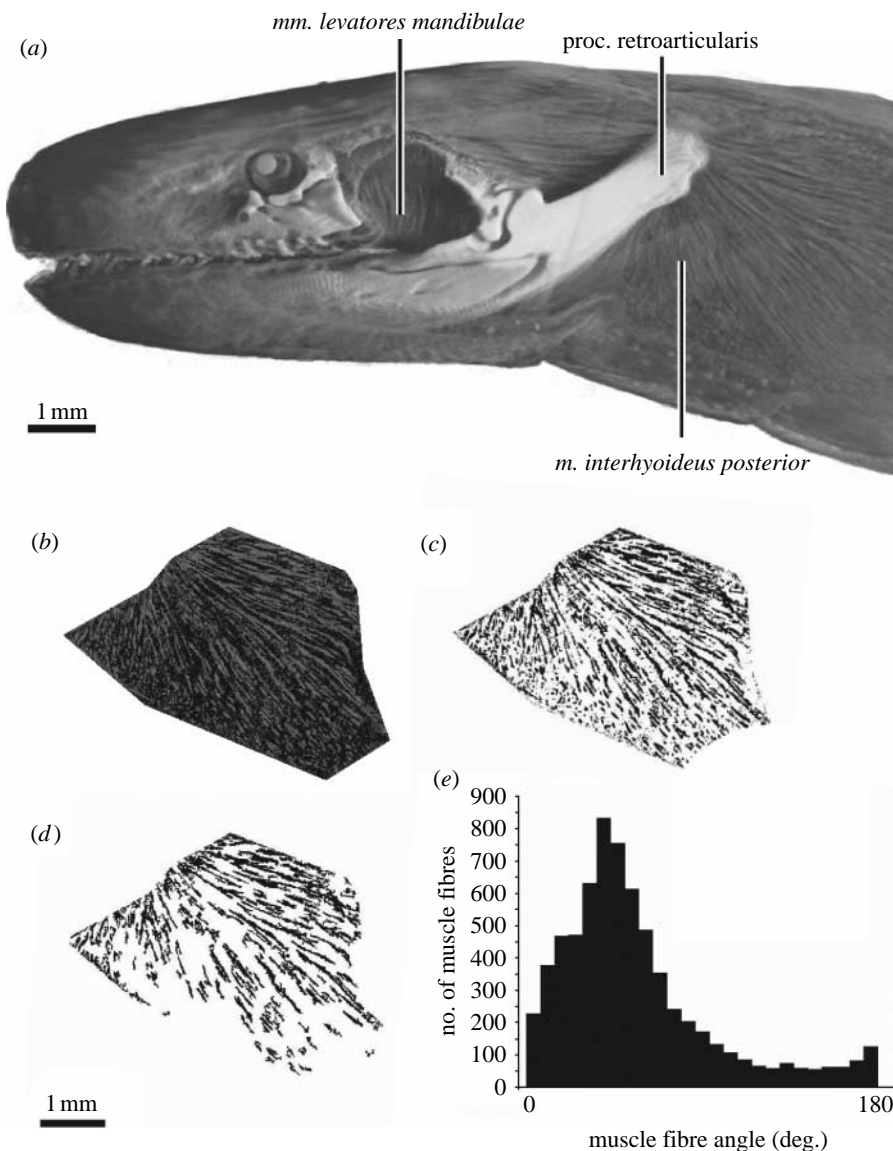
Figure 3. A method for measuring muscle fibre angle from high resolution, synchrotron-based X-ray CT scan data. (*a*) A volume rendering of the CT image data for *I.* cf. *kohtaoensis* shown in lateral view with the skin removed to reveal the underlying skeleton and muscles. The squamosal bone has also been removed to show the levator mandibulae muscle complex. (*b*) A contrast enhanced, grey-scale image of a parasagittal section of the IHP from the CT image data. (*c*) The section in (*b*) thresholded to emphasize the muscle fibres. (*d*) The section shown in (*c*) with all connected areas smaller than 25 pixels in area removed, and all areas with a circularity of more than 0.3 removed. The remaining areas are muscle fibres with measurable angles. (*e*) Histogram showing the distribution of angular measurements for the 6797 fibres measured from the image stack for the IHP from the left side of *I.* cf. *kohtaoensis* that included image (*b*). Count 6797, mean 44.61 (56.24), s.d. 32.08, min. $-41.98°$ (0°), max. 137.93 (180°).

of the cranial bones, we produced physical models of the caecilian skulls including the lower jaws on a ZPrinter 310 rapid prototyping machine (ZCorp, Burlington, MA). The models were based on the CT datasets. We segmented the quadrate–squamosal complex, the pterygoid and the stapes on the right-hand side of the skull with AMIRA v. 4.1 in order to produce separated models for those parts. The resulting physical models are scaled up in size (*I.* cf. *kohtaoensis* and *T. natans* scale factor: 14.5; *S. annulatus* scale factor: 10.7) compared to the skulls in the specimens. The physical models were manipulated by hand to estimate the degrees of lower jaw and quadrate–squamosal movements. We then used MAYA v. 6.0 to animate the VRML dataset of the *I.* cf. *kohtaoensis* specimen. The computer animation is based on the results of the interaction with the physical model for this species. The movie files of the animation are available as information in the electronic supplementary material.

3. RESULTS

All measurements used for the calculations of EMAs and bite forces over gape angles are listed in table 2. The ratios of the lengths of the in-lever to out-lever for the *mm. levatores mandibulae* range from 0.055 (*m. levator mandibulae articularis* in *S. annulatus*) to 0.264 (*m. levator mandibulae longus* in *T. natans*). The lever arm ratios are higher for the IHP in all the three investigated species: 0.404 in *I.* cf. *kohtaoensis*; 0.58 in *S. annulatus*; and 0.538 in *T. natans*.

Table 2. Measurements of functionally important anatomical characters and calculation of maximal force of single muscles for the three investigated species.

		Ichthyophis cf. *kohtaoensis*	*Siphonops annulatus*	*Typhlonectes natans*
m. levator mandibulae articularis	length in-lever l_{LEV} (mm)	0.775	0.575	0.635
	l_{LEV}/l_{LJ}	0.100	0.055	0.093
	fibre angle β_{LMA} (°)	88.3 ± 24.7	97.2 ± 30.6	88.0 ± 34.7
	volume (mm^3)	0.695	0.424	0.304
	length (mm)	1.699	1.999	1.181
	volume/length (mm^2)	0.409	0.212	0.257
	force (N)	0.102	0.053	0.064
m. levator mandibulae internus	length in-lever l_{LEV} (mm)	1.655	2.105	1.805
	l_{LEV}/l_{LJ}	0.214	0.200	0.264
	fibre angle β_{LMA} (°)	116.1 ± 29.7	102.5 ± 32.6	125.5 ± 32.0
	volume (mm^3)	1.385	6.860	0.819
	length (mm)	2.296	4.214	2.772
	volume/length (mm^2)	0.603	1.628	0.295
	force (N)	0.151	0.407	0.074
m. levator mandibulae longus	length in-lever l_{LEV} (mm)	1.655	2.105	1.805
	l_{LEV}/l_{LJ}	0.214	0.200	0.264
	fibre angle β_{LMA} (°)	91.5 ± 27.8	96.6 ± 31.3	79.2 ± 35.4
	volume (mm^3)	1.195	4.025	2.685
	length (mm)	2.433	3.981	2.941
	volume/length (mm^2)	0.491	1.011	0.913
	force (N)	0.123	0.252	0.228
m. interhyoideus posterior	length in-lever l_{RP} (mm)	3.120	6.100	3.680
	l_{RP}/l_{LJ}	0.404	0.580	0.538
	fibre angle ε (°)	41.2 ± 30.9	36.2 ± 31.4	57.3 ± 28.2
	volume (mm^3)	22.400	30.600	12.100
	length (mm)	5.135	7.294	5.687
	volume/length (mm^2)	4.363	4.195	2.128
	force (N)	1.09	1.05	0.53
length out-lever lower jaw l_{LJ} (mm)		7.718	10.525	6.840
angle processus retroarticularis γ (°)		32.7	16.8	22.3
angle quadrate–squamosal complex δ (°)		26.0	27.5	26.2

Average muscle fibre angle orientations of the *levator mandibulae* complex relative to the anteroposterior axis range from 79.2° (*m. levator mandibulae longus* in *T. natans*) to 125.5° (*m. levator mandibulae internus* in *T. natans*). The fibres of the IHP are oriented on average 41.2° in *I.* cf. *kohtaoensis*, 36.2° in *S. annulatus* and 57.3° in *T. natans*.

The *m. levator mandibulae articularis* has the smallest ratio of muscle volume to muscle length (PCSA) in all the investigated specimens. The PCSA values of the *m. levator mandibulae articularis* are between 0.212 (*T. natans*) and 0.409 mm^2 (*I.* cf. *kohtaoensis*). The PCSA value ranges from 0.295 (*T. natans*) to 1.628 mm^2 (*S. annulatus*) for the *m. levator mandibulae internus* and from 0.491 (*I.* cf. *kohtaoensis*) to 1.011 mm^2 (*S. annulatus*) for the *m. levator mandibulae longus*. In the three investigated caecilian species, the IHP has the largest PCSA value of all muscles: 4.363 mm^2 in *I.* cf. *kohtaoensis*; 4.195 mm^2 in *S. annulatus*; and 2.128 mm^2 in *T. natans*.

Calculated maximal bite forces range from 0.053 (*m. levator mandibulae articularis* in *T. natans*) to 0.407 N (*m. levator mandibulae internus* in *S. annulatus*) for the *levator mandibulae* group and from 0.53 (*T. natans*) to 1.09 N (*I.* cf. *kohtaoensis*) for the IHP.

The retroarticular process of the lower jaw is angled 32.7° dorsally in *I.* cf. *kohtaoensis*, 16.8° in *S. annulatus* and 22.3° in *T. natans* with respect to the anteroposterior axis. The quadrate–squamosal complex is oriented at 26° to the anteroposterior axis in *I.* cf. *kohtaoensis*, 27.5° in *S. annulatus* and 26.2° in *T. natans*.

3.1. Effective mechanical advantage and gape angle

The EMAs of all *mm. levatores mandibulae* are maximal at a closed lower jaw in all the investigated species (figure 4; table 3). With increasing gape angle, the EMA of the *mm. levatores mandibulae* decreases. The muscles of the levator mandibulae group in the investigated species have critical values for gape angles above which the EMAs become negative (figure 4). Critical gape angles range from 64.4° (*m. levator mandibulae articularis* in *S. annulatus*) to 84.8° (*m. levator mandibulae internus* in *T. natans*; table 3).

The EMA of the IHP in the three investigated species increases with increasing gape angle, reaches a maximum value at gape angles of 55.2° (*I.* cf. *kohtaoensis*), 51.8° (*S. annulatus*) and 78.3° (*T. natans*), and decreases with increasing gape angles above the optimal gape
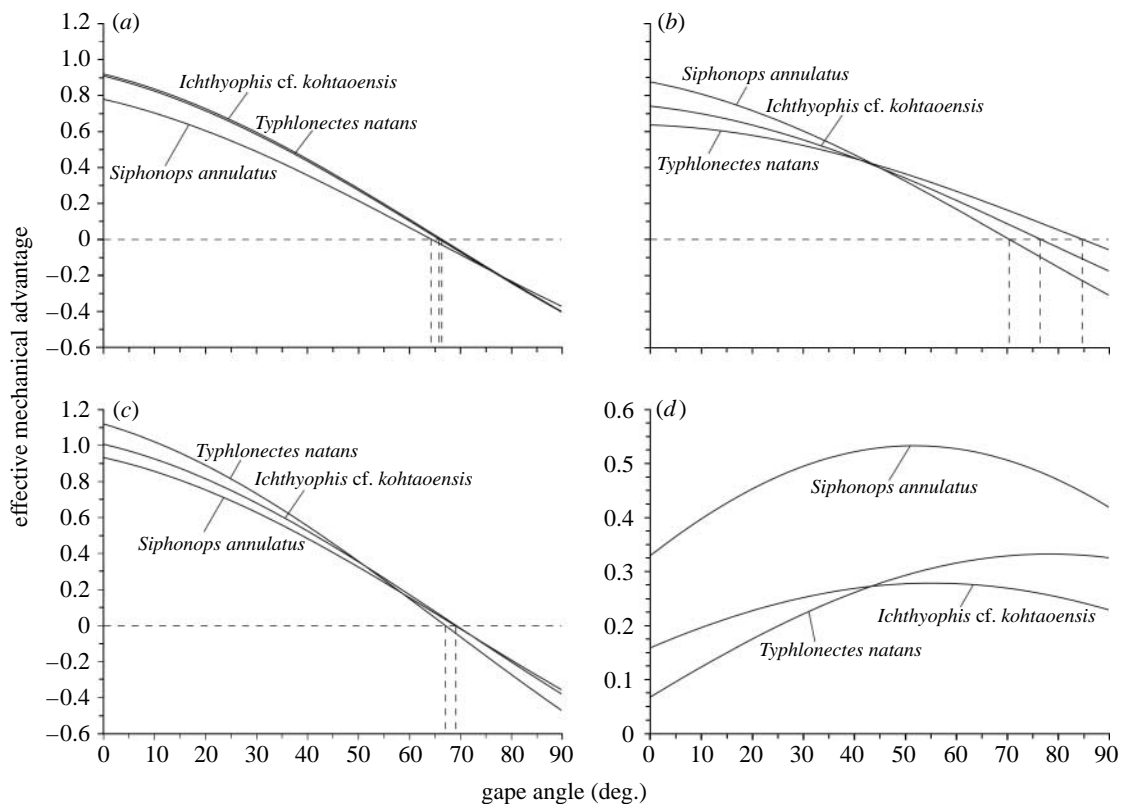
Figure 4. The EMA of each of the jaw-closing muscles for three species of caecilians, *I.* cf. *kohtaoensis*, *S. annulatus* and *T. natans*: (*a*) *m. levator mandibulae articularis*, (*b*) *m. levator mandibulae internus*, (*c*) *m. levator mandibulae longus*, (*d*) IHP. This is the amount of amplification of the actual muscle force that will appear at the tip of the lower jaw. At an EMA greater than 0 the muscle tends to close the jaw, and at an EMA less than 0 it tends to pull the jaw open. This critical gape angle, where EMA = 0 varies by species and is not seen for the IHP. This illustrates that some architectures are force amplifiers. At small gape angles, the *m. levator mandibulae longus* can have an EMA greater than 1, which means that the force at the tip of the jaws exceeds the force generated by the jaw muscle. The maximum EMA of the three adductor muscles is when the jaws are closed, whereas for the IHP, there is a peak EMA between 50° and 80° gape angle.

(figure 4; table 3). None of the investigated species shows a critical gape angle for the IHP.

Maximal EMAs of the *mm. levatores mandibulae* range from 0.64 (*m. levator mandibulae internus* in *T. natans*) to 1.12 (*m. levator mandibulae longus* in *T. natans*). The maximal EMA values of the IHP are lower than that of the *levator mandibulae* group; they range between 0.28 (*I.* cf. *kohtaoensis*) and 0.53 (*S. annulatus*; table 3).

3.2. Bite force and gape angle

In the three investigated species, the *mm. levatores mandibulae* contribute best to total bite force (i.e. the sum of bite forces from all the jaw-closing muscles) at a closed lower jaw. The *mm. levatores mandibulae*-generated forces decrease with increasing gape angle, i.e. when the jaw opens. The force output of the IHP increases with wider gape angles (figure 5) until it reaches a maximum value. Total bite force is almost constant at small gape angles (0°–30°) and decreases with higher gape angles (figure 5).

In *I.* cf. *kohtaoensis*, the calculated forces for the *mm. levatores mandibulae* for one side of the body with a closed lower jaw are 0.094 (*m. levator mandibulae articularis*), 0.111 (*m. levator mandibulae internus*) and 0.124 N (*m. levator mandibulae longus*; table 4). The IHP contributes 0.174 N to the bite force when the

jaws are closed; the calculated maximum value is 0.305 N at a gape angle of 55° (figure 5; table 4). The bilateral sum of all muscles shows a maximum total bite force of 1.045 N at a gape angle of 16° (table 4).

In *S. annulatus*, the *m. levator mandibulae articularis* contributes 0.041 N, the *m. levator mandibulae internus* 0.355 N, the *m. levator mandibulae longus* 0.235 N and the IHP 0.347 N to the estimated bite force when the jaws are closed (table 4). The IHP reaches a maximal force value of 0.557 N at a gape angle of 55°. The calculated total bite force for both sides of the body is maximal at a gape angle of 13° when the animal can exert 2.0 N.

In *T. natans*, we calculated for the *mm. levatores mandibulae* bite forces at a closed lower jaw of 0.059 (*m. levator mandibulae articularis*), 0.048 N (*m. levator mandibulae internus*) and 0.255 N (*m. levator mandibulae longus*). The IHP contributes 0.037 N to the estimated total bite force at zero gape (table 4). The maximum bite force of 0.173 N is generated by the IHP at a gape angle of 78°. The total bite force for all the muscles on both sides of the head was calculated with a maximum value of 0.796 N at a gape angle of 6° (table 4).

3.3. Impact of different fibre orientations

The standard deviation for the values of muscle fibre angles range from 24.7° (*m. levator mandibulae*

Table 3. Calculations of effective mechanical advantages (EMA) and functionally important gape angles (α) for single muscles. (Results shown for calculations with mean muscle fibre angles ($\beta_{mean}/\varepsilon_{mean}$), minimal fibre angles ($\beta_{min}/\varepsilon_{min}$) and maximal fibre angles ($\beta_{max}/\varepsilon_{max}$).)

	Ichthyophis cf. kohtaoensis			Siphonops annulatus			Typhlonectes natans		
	EMA max β_{mean} (β_{min}; β_{max})	α max [°] β_{mean} (β_{min}; β_{max})	critical $\alpha=0°$ β_{mean} (β_{min}; β_{max})	EMA max β_{mean} (β_{min}; β_{max})	α max [°] β_{mean} (β_{min}; β_{max})	critical $\alpha=0°$ β_{mean} (β_{min}; β_{max})	EMA max β_{mean} (β_{min}; β_{max})	α max [°] β_{mean} (β_{min}; β_{max})	critical $\alpha=0°$ β_{mean} (β_{min}; β_{max})
m. levator mandibulae articularis	0.92 (0.99; 0.68)	0 (0; 0)	66 (64; 70)	0.78 (0.93; 0.41)	0 (0; 0)	66 (63; 69)	0.91 (0.95; 0.54)	0 (0; 0)	66 (63; 72)
m. levator mandibulae internus	0.74 (1.04; 0.27)	0 (0; 24)	76 (68; —)	0.87 (1.07; 0.41)	0 (0; 1)	70 (64; —)	0.64 (1.04; 0.27)	0 (0; 81)	85 (70; —)
m. levator mandibulae longus	1.01 (1.09; 0.69)	0 (0; 0)	69 (64; 78)	0.93 (1.07; 0.53)	0 (0; 0)	69 (63; 83)	1.12 (1.02; 0.80)	0 (0; 0)	67 (59; 78)
	EMA $\alpha=0°$ ε_{mean} (ε_{min}; ε_{max})	α max [°] ε_{mean} (ε_{min}; ε_{max})	ε_{mean} (ε_{min}; ε_{max})	EMA $\alpha=0°$ ε_{mean} (ε_{min}; ε_{max})	α max [°] ε_{mean} (ε_{min}; ε_{max})	ε_{mean} (ε_{min}; ε_{max})	EMA $\alpha=0°$ ε_{mean} (ε_{min}; ε_{max})	α max [°] ε_{mean} (ε_{min}; ε_{max})	ε_{mean} (ε_{min}; ε_{max})
m. interhyoideus posterior	0.28 (0.55; 0.21)	55 (19; 90)	0.16 (0.52; −0.25)	0.53 (0.66; 0.35)	52 (33; 89)	0.33 (0.56; 0.01)	0.33 (0.52; 0.21)	78 (44; 90)	0.07 (0.38; −0.26)

articularis in *I.* cf. *kohtaoensis*) to 35.4° (*m. levator mandibulae longus* in *T. natans*; table 2). EMAs and thus bite forces increase with smaller values for muscle fibre angles in all the investigated species and muscles; larger fibre angles decrease EMA and bite force (tables 3 and 4).

The gape angle at which the muscles have their best EMA increases with increasing fibre angle (table 3) for the *m. levator mandibulae internus* and the IHP, and thus variation in fibre orientation has an effect on total bite force over gape angle (table 4).

The critical gape angles increase with increasing fibre angle for all the muscles. For the *m. levator mandibulae internus*, the increase in critical gape angle results in a critical gape that is beyond the maximal gape angle considered herein (90°; table 3).

3.4. Rapid prototyping and animation

The scaled-up, rapid prototyped models of the lower jaw clearly show a partially captured mandibular joint (figure 6a,d,g) in that the fossa of the jaw joint in the *pseudoangular* is a deep mediocaudally oriented ridge (figure 6c,f,i) that wraps around the condyle of the *quadrate*. Interactive manipulation of the rapid prototyped models and the resulting three-dimensional computer animation (see information in the electronic supplementary material) show substantial dorsolateral movement of the quadrate–squamosal complex as the lower jaw closes. This movement is driven by the mediocaudally oriented fossa of the lower jaw, which necessitates some degree of lateral movement of the lower jaw as the jaw opens (figure 7; see information in the electronic supplementary material).

4. DISCUSSION

Our analysis of the caecilian jaw function has brought to light several interesting features of these unusual amphibians. When the gape angle exceeds some critical angle, the force generated by one set of jaw muscles transitions from closing the jaws to opening them (figure 4). The previous model of jaw function did not predict this because it did not account for the fibre orientation of the muscles, realistic orientations of the quadrate–squamosal complex or the levator muscle complex (Summers & Wake 2005). The critical gape angle has two important consequences: first, as gape increases the contribution of the levator complex will decrease (figures 4 and 5); and second, the forces oriented at oblique angles relative to the long axis of the jaw are one set that will tend to destabilize the jaw joint. Our model suggests that at gape angles higher than approximately 70°, the *mm. levatores mandibulae* will open the lower jaw and thus counteract to the IHP. Although the IHP has its peak mechanical advantage at rather high gape angles (table 3; figure 4) and thus has the potential to compensate for the *mm. levatores mandibulae*, this theoretical scenario seems to be of little biological relevance. The gape angle data are available from *I. kohtaoensis*, *T. natans* and *Hypogeophis rostratus*, which show peak gape angles of not more than 60° (O'Reilly 2000). This coincides with our model
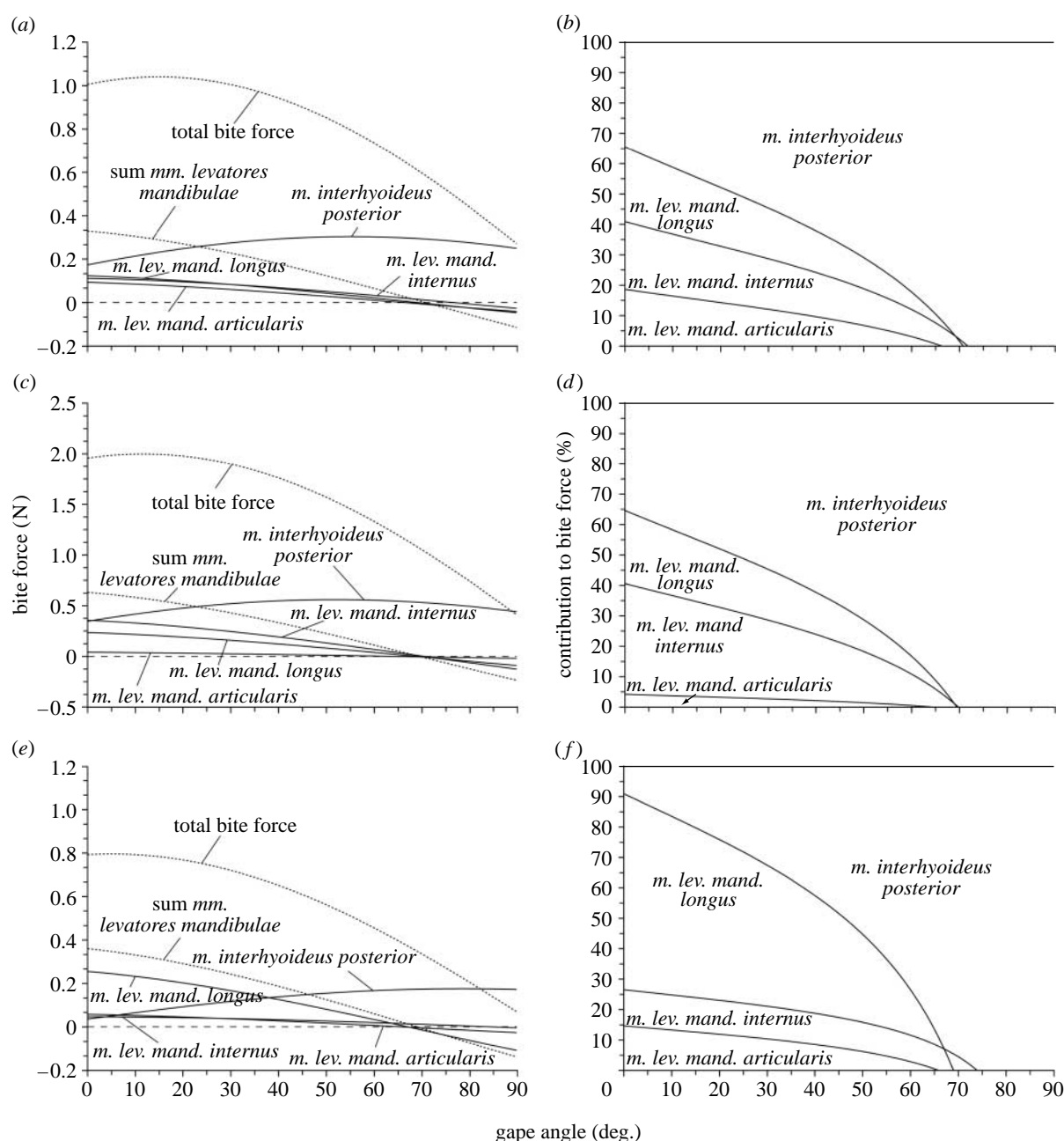
Figure 5. Modelled bite forces at varying gape angles for three species of caecilians: (*a*,*b*) *I.* cf. *kohtaoensis*, (*c*,*d*) *S. annulatus* and (*e*,*f*) *T. natans*. (*a*,*c*,*e*) Absolute force generated by the four jaw-closing muscles and the sum of the forces of the three *mm. levatores mandibulae* as well as the total bite force as sum of all four muscles for both sides of the skull. (*b*,*d*,*f*) The relative contributions of single muscles (for both skull sides) to the total bite force.

predictions that critical gape angles for single muscles of the *mm. levatores mandibulae* are at approximately 65° for the three investigated species (table 3; figure 4).

The synchrotron-based X-ray radiation CT image data made it possible to measure fibre angles for a large number of fibres relative to the methods that rely on a dissecting scope and goniometer (thousands versus dozens) in a reasonable investment of time. However, the technique may also introduce errors. These fall into two categories, those which affect the measurement of cross-sectional area and those which affect the angles measured. Two sources of error are apparent, the first is that the specimen must be freeze dried in order to visualize the soft tissues clearly and the second is that the method we developed is two dimensional, whereas

the muscles are three-dimensional structures. We do not suppose that the estimation of volume from the freeze-dried specimens is very different from that which would be obtained from fresh material. Shrinkage that occurs during the fixation of specimens in formalin and storage in ethanol usually decreases the volume by approximately 20–25% (Böck 1989). However, most of this shrinkage (approx. 20%; Böck 1989) is caused by dehydration, which was at least partially compensated by rehydration of the specimens prior to freeze drying. Freeze drying itself is known to reduce the volume by approximately 15% (Boyde 1978). Thus, we estimate the volume shrinkage due to fixation and drying to not more than approximately 25%. Bite force would then be underestimated by approximately 17%. We virtually

Table 4. Calculated maximum bite force values and bite forces at a closed lower jaw for cranial muscles in the three investigated species. (Results shown for calculations with mean muscle fibre angles (β_{mean}), minimal fibre angles (β_{min}) and maximal fibre angles (β_{max}).)

	Ichthyophis cf. *kohtaoensis*			*Siphonops annulatus*			*Typhlonectes natans*		
	force $\alpha=0$ [N]	force max [N]	α max [°]	force $\alpha=0$ [N]	force max [N]	α max [°]	force $\alpha=0$ [N]	force max [N]	α max [°]
	β_{mean} (β_{min}; β_{max})	β_{mean} (β_{min}; β_{max})	β_{mean} (β_{min}; β_{max})	β_{mean} (β_{min}; β_{max})	β_{mean} (β_{min}; β_{max})	β_{mean} (β_{min}; β_{max})	β_{mean} (β_{min}; β_{max})	β_{mean} (β_{min}; β_{max})	β_{mean} (β_{min}; β_{max})
m. levator mandibulae articularis	0.09 (0.10; 0.07)	0.09 (0.10; 0.07)	0 (0; 0)	0.04 (0.05; 0.02)	0.04 (0.05; 0.02)	0 (0; 0)	0.06 (0.06; 0.04)	0.06 (0.06; 0.04)	0 (0; 0)
m. levator mandibulae internus	0.11 (0.16; 0.04)	0.11 (0.16; 0.04)	0 (0; 24)	0.35 (0.43; 0.17)	0.35 (0.43; 0.17)	0 (0; 1)	0.05 (0.08; 0.00)	0.05 (0.08; 0.02)	0 (0; 81)
m. levator mandibulae longus	0.12 (0.13; 0.09)	0.12 (0.13; 0.09)	0 (0; 0)	0.23 (0.27; 0.13)	0.23 (0.27; 0.13)	0 (0; 0)	0.25 (0.23; 0.18)	0.25 (0.23; 0.18)	0 (0; 0)
m. interhyoideus posterior	0.17 (0.57; −0.27)	0.31 (0.60; 0.23)	55 (19; 90)	0.35 (0.59; 0.01)	0.56 (0.70; 0.37)	52 (33; 89)	0.04 (0.20; −0.14)	0.17 (0.28; 0.11)	78 (44; 90)
sum *mm. levatores mandibulae*	0.33 (0.39; 0.19)	0.33 (0.39; 0.19)	0 (0; 0)	0.63 (0.75; 0.32)	0.63 (0.75; 0.32)	0 (0; 0)	0.36 (0.37; 0.22)	0.36 (0.37; 0.22)	0 (0; 0)
total bite force	1.00 (1.92; −0.16)	1.05 (1.92; 0.41)	16 (1; 90)	1.96 (2.67; 0.65)	2.00 (2.67; 0.95)	13 (0; 47)	0.79 (1.14; 0.17)	0.80 (1.14; 0.24)	6 (0; 45)

sectioned the three-dimensional muscle volume in a plane that was as nearly parallel to the fibre direction as we could estimate from a lateral projection. The distribution of fibre angles (figure 3e) suggests that we have successfully estimated the orientations from muscle fibres and the mean fibre angle. Furthermore, figure 3c shows all the potential fibres and when compared with figure 3d, which shows only the measured fibres, it is clear that we have managed to section in a plane parallel to the majority of the fibres. The most extreme fibre angles that were derived from standard deviation values within the sample can result in a different behaviour of the model (tables 3 and 4). *In vivo* it seems also possible that muscle fibres change their orientation during shortening, an effect that is not considered herein. However, based on the distribution of fibre angles (figure 3e), we suggest that the average value of fibre angle is a decent estimation to interpret muscle function. Most of the fibres have an average fibre orientation and higher and lower values for muscle fibre angles seem likely to outweigh each other in the animal. Literature estimates of fibre directions are also made from two-dimensional projections of the muscles and owing to the laborious nature of making angular measurements by hand are always on a very small subset of muscle fibres. We suggest that the synchrotron method yields results that are more representative of the actual muscle architecture and it has the advantage of being able to be extended into true three dimensionality.

The unusual, partially captive rotating joint of the lower jaw of caecilians (figure 6) could be explained by two factors. Consider the force generated by the jaw muscles. There is a component of this force perpendicular to the jaw or retroarticular process that closes the gape. Another component, parallel to the jaw, tends to dislocate the jaw joint. The existence of a critical angle implies that as the gape increases the component perpendicular to the jaws decreases, therefore the parallel component of the muscle force will increase. So, with increasing gape, there is a greater force tending to dislocate the jaws. The IHP itself, because it acts on the opposite side of the jaw than the *levator mandibulae* complex, will exert tension to the mandibular joint. This force tends to loose the connection between lower jaw and jaw joint. The way in which the mandibular fossa of the lower jaw is wrapped around the condyle of the articular bone stabilizes the joint against these forces. An analogue for this joint is seen in mammal carnivores (particularly the mustelids), in which the condylar process of the mandible is captured by the squamosal bone (Scapino 1976, 1981; Radinsky 1982; Riley 1985). Besides the skeletal features, the *m. pterygoideus* (innervated by cranial nerve V) seems likely to stabilize the mandibular joint as well.

Every jaw-closing muscle has its own critical angle, and the two sets of jaw closers have quite different average critical angles—this means that for any biologically relevant gape, there is some muscle in one of the two systems that can exert a closing force. An implication of the different critical angles is that the contribution of single muscles to closing force will vary with gape angle. For example, in *I.* cf. *kohtaoensis* at a gape of 10° the *mm. levatores mandibulae* contribute
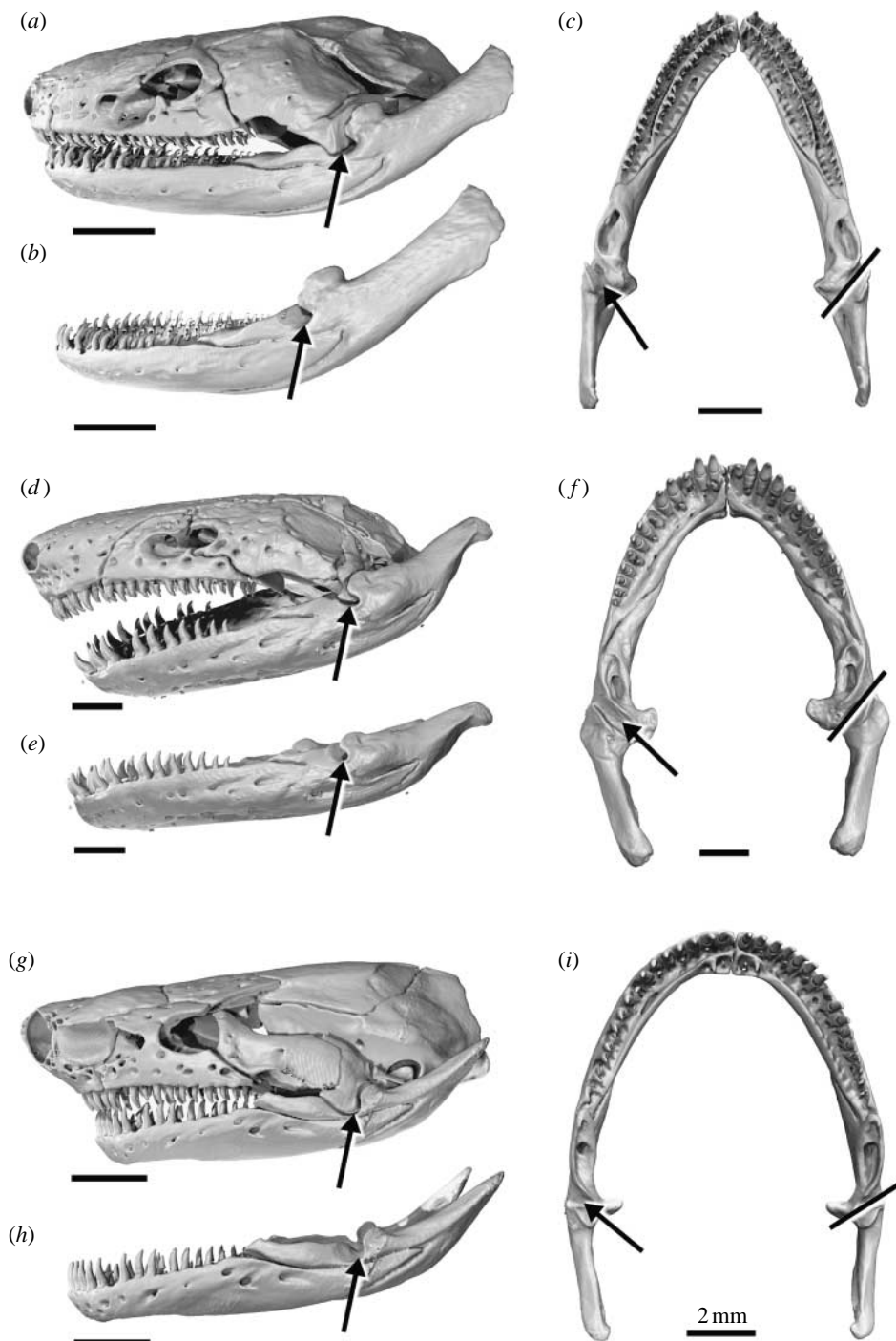
Figure 6. Anatomy of the mandibular joint in three species of caecilians: (*a–c*) *I.* cf. *kohtaoensis*, (*d–f*) *S. annulatus* and (*g–i*) *T. natans* reconstructed from CT image data. Surface renderings of the skull and lower jaw in lateral view (*a,d,g*) showing the articulation between the pseudoangular and the quadrate (arrow). The disarticulated lower jaw showing the deep groove of the mandibular fossa (*b,e,h*). Dorsal views of the lower jaws (*c,f,i*) showing the fossa on the left side (arrow) and tracing its oblique orientation on the right side (solid line).

approximately 60% of the total closing force, whereas when the mouth is open to 50° they contribute only 35%. The net effect of this variation is that as the force from the *mm. levatores mandibulae* is decreasing, the force of the second jaw-closing system, the IHP, is increasing and the total force exerted at the tips of the jaws is similar over a wide range of gape. If we consider the jaw-closing force of all the three caecilians between 0° and 35° gape angles, the closing force varies by less than 10% from its peak value (figure 5), and over the most extreme gape angles (approx. 60°) seen in the

literature the force drops just 29 (*I.* cf. *kohtaoensis*), 33 (*S. annulatus*) or 43% (*T. natans*) from the peak. Maintaining high closing forces over a wide range of gapes seems important for dietary generalists, such as these three species (Moodie 1978; Gudynas *et al.* 1988; Verdade *et al.* 2000; Presswell *et al.* 2002; Kupfer & Maraun 2003; Gaborieau & Measey 2004; Measey *et al.* 2004; Kupfer *et al.* 2005).

These theoretical models of bite force have proven quite robust relative to measured bite force in a wide variety of organisms (Herrel *et al.* 1998, 2002;
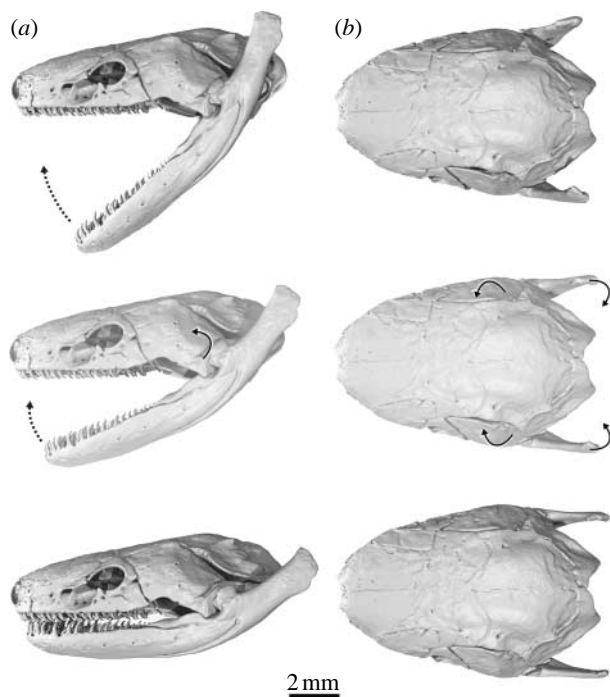
Figure 7. Movements of the quadrate–squamosal complex in *I.* cf. *kohtaoensis* reconstructed from CT image data and based on interactive manipulation of rapid prototyped skulls. Surface renderings of the skull and lower jaw: (*a*) lateral and (*b*) dorsal views. The anatomy of the mandibular joint causes a mediolateral movement of the lower jaw, during opening and closing movements. The mediolateral movement is compensated by movements of the quadrate–squamosal complex.

Greaves 2000; Westneat 2003; Herrel & Aerts 2004; Huber & Motta 2004; Huber *et al.* 2005) and there is some evidence to suggest that our model is also close to measured caecilian bite force. Models of bite force based on the geometry and the PCSA of muscle often underestimate the actual forces measured during biting *in vivo* (Herrel *et al.* 1998, 2008; Meyers *et al.* 2002; but see Huber *et al.* 2005). This may be because the models typically do not take into account all of the potential jaw closers, or more probably the models ignore the effects of non-closing muscles on bite force. When bite forces are measured with a force transducer, the animal has some contact with either the substrate or the experimenter and has the opportunity to exploit the effects of trunk musculature to aid in jaw closure. The two experimentally determined bite forces for caecilians are 0.62 and 1.09 N for *Boulengerula taitanus* and *Schistometopum thomense* (Measey & Herrel 2006)—comparable values to our calculated peak forces (0.8–2.0 N). However, our values are proportionally lower in light of the size of our three individuals relative to the substantially smaller animals in the experimental study. The bite forces from similar-sized animals are quite a bit higher (approx. 3–6 N; A. Herrel 2007, personal communication). The difference between our theoretical values and the measured forces might be explained as an effect of the animals recruiting body musculature, in this case vertebral muscles, to augment the levator and IHP systems. This is supported by the activation of trunk musculature during the static

pressure phase of the caecilian bite cycle as shown electromyographically by Bemis *et al.* (1983). Further, the caecilians will spin about their long axis, using this rotational movement to shear prey against the sides of their burrow or to determine its size (Measey & Herrel 2006).

Streptostyly, the mobile joint between the quadrate–squamosal and the neurocranium, seems at odds with the otherwise tightly fused caecilian skull—we propose two advantages to this architecture: first, streptostyly compensates for the lateral movements of the lower jaw; and second, the rotational movement of the quadrate–squamosal contributes additionally to bite force by shortening the distance between lower and upper jaws.

When we produced the oversized prototypes of skulls and jaws from the CT scan data, it became clear that the joint between the lower jaw and the quadrate–squamosal has a very limited range of motion. Rather than the loose saddle joint we had expected, the quadrate–squamosal is firmly captured in a groove of the pseudoangular, and is a rotational joint with very little mobility off the rotational axis (figure 6). Because the axis of the mandibular joint is not perpendicular to the long axis of the lower jaw, to open the mouth the lower jaw will rotate downwards and laterally. The lateral movement of the lower jaw must be compensated for by a lateral rotation of the quadrate–squamosal (figure 7; see information in the electronic supplementary material). The two bones of the lower jaw, i.e. pseudodentary and pseudoangular, share a rather loose suture and there seems to be potential for intramandibular mobility. If true, movements within the lower jaw could be related to the lateral component during jaw closure. As an aside, the deep groove in the pseudoangular (figure 6) was previously mentioned by Wiedersheim (1879) who interprets this structure as comparable to the jaw joint in teleosts or lungfishes, and Marcus *et al.* (1933) who believed that the deep groove tightens the mandibular joint during the action of the *m. pterygoideus*. We suggest that this tight joint is an adaptation to the two forces that tend to dislocate the jaw during feeding.

Another advantage of streptostyly is highlighted by the high EMA of the levators. The second mobile joint of the jaws forms an unusual lever system that converts some of the force that tends to dislocate the lower jaw into a closing force. This streptostyly-based closing force is due to the upward rotation of the quadrate–squamosal (and thus the mandibular joint itself), which moves the lower jaw towards the upper jaw. The streptostyly component of bite force is added to the force that results from the regular closing movement of the lower jaw. This mechanism amplifies the mechanical advantage of the levators in particular, though it also helps the IHP system (Summers & Wake 2005). In both *I.* cf. *kohtaoensis* and *T. natans* one of the levators, the *m. levator mandibulae longus*, has an EMA greater than 1. This means that despite inserting rather close to the jaw joint it exerts as much, or even a little more, force at the tips of the jaws than it develops at its insertion. Indeed, it had been proposed that the muscles of the *levator mandibulae* group are so close to the joint that they

might be adapted for high-speed closure of the jaws (Summers & Wake 2005); we find instead that like the IHP they are well suited to exerting large forces on prey.

An interesting connection to skull architecture comes from understanding the *mm. levatores mandibulae* as important contributors to bite force. Many caecilian skulls, including two of the species we looked at here, are stegokrotaphic; that is, the temporal region of the skull is roofed with bone. By contrast, *T. natans* is zygokrotaphic—there is a significant opening between the squamosal and the parietal bones, which leaves substantially more room for jaw levator muscles. This architectural difference is reflected in the relative contributions to force of the two jaw adductor systems to closing force. In the two stegokrotaphic species, the levators contribute approximately 65–42% of the total force at gapes from 0° to 35°, but in the zygokrotaphic species these same muscles contribute approximately 91–64% at the same gape angles. We attribute this difference to the zygokrotaphic species being able to pack more muscle, with better lever arms, into the skull than can the two species with the roofed temporal region. It is tempting to extrapolate further from this small dataset, perhaps into the realm of ecology, where *T. natans* is an aquatic animal, while both *I.* cf. *kohtaoensis* and *S. annulatus* are terrestrial and fossorial. However, with the confounding effects of phylogeny and ecology and the very limited sample size used for our study, there is nothing that can be said at the moment. If a large contribution from the *mm. levatores mandibulae* is characteristic of aquatic feeding, we might expect to see similar force contribution patterns in those species of caecilians with aquatic larvae (i.e. Rhinatrematidae, Ichthyophiids, Uraeotyphlidae and some Caeciliidae). There is also an opportunity to further our understanding by examining an independent radiation of zygokrotaphic but terrestrial caecilians, i.e. the Scolecomorphidae.

REFERENCES

Bemis, W. E., Schwenk, K. & Wake, M. H. 1983 Morphology and function of the feeding apparatus in *Dermophis mexicanus* (Amphibia: Gymnophiona). *Zool. J. Linn. Soc.* **77**, 75–96.

Biewener, A. A. 1989 Scaling body support in mammals: limb posture and muscle mechanics. *Science* **245**, 45–48. (doi:10.1126/science.2740914)

Böck, P. 1989 *Romeis mikroskopische Technik*, p. 697. Baltimore, MD: Urban und Schwarzenberg.

Boyde, A. 1978 Pros and cons of critical point drying and freeze drying for SEM. *Scan. Electron. Microsc.* **2**, 303–314.

De Villiers, C. G. S. 1936 Some aspects of the Amphibian suspensorium, with special reference to the paraquadrate and quadratomaxillary. *Anat. Anz.* **81**, 225–247.

Edgeworth, F. H. 1935 *The cranial muscles of vertebrates*, p. 493. London, UK: Cambridge University Press.

Frost, D. R. 2007 *Amphibian species of the world: an online reference*, version 5.1 (10 October 2007). New York, NY: American Museum of Natural History. Electronic database accessible at http://research.amnh.org/herpetology/amphibia/index.php.

Frost, D. R. *et al.* 2006 The amphibian tree of life. *Bull. Am. Mus. Nat. Hist.* **297**, 1–370. (doi:10.1206/0003-0090(2006)297[0001:TATOL]2.0.CO;2)

Gaborieau, O. & Measey, G. J. 2004 Termitivore or detritivore? A quantitative investigation into the diet of the East Arican caecilian *Boulengerula taitanus* (Amphibia: Gymnophiona: Caeciliidae). *Anim. Biol. Leiden Neth.* **54**, 45–56. (doi:10.1163/157075604323010042)

Gower, D. J. *et al.* 2002 A molecular phylogeny of ichthyophiid caecilians (Amphibia: Gymnophiona: Ichthyophiidae): out of India or out of South East Asia? *Proc. R. Soc. B* **269**, 1563–1569. (doi:10.1098/rspb.2002.2050)

Greaves, W. S. 2000 Location of the vector of jaw muscle force in mammals. *J. Morphol.* **243**, 293–299. (doi:10.1002/(SICI)1097-4687(200003)243:3<293::AID-JMOR6>3.0.CO;2-5)

Gudynas, E., Williams, J. D. & De Las Mercedes Azpelicueta, M. 1988 Morphology, ecology, and biogeography of the South American caecilian *Chthonerpeton indistinctum* (Amphibia: Gymnophiona: Typhlonectidae). *Zoologische Mededelingen* **62**, 5–28.

Haas, A. 2001 Mandibular arch musculature of anuran tadpoles, with comments on homologies of amphibian jaw muscles. *J. Morphol.* **247**, 1–33. (doi:10.1002/1097-4687(200101)247:1<1::AID-JMOR1000>3.0.CO;2-3)

Herrel, A. & Aerts, P. 2004 Biomechanical studies of food and diet selection. In *Encyclopedia of life sciences*. Chichester, UK: Wiley. See http://www.els.net/. (doi:10.1038/npg.els.0003213)

Herrel, A., Aerts, P. & De Vree, F. 1998 Ecomorphology of the lizard feeding apparatus: a modelling approach. *Neth. J. Zool.* **48**, 1–25. (doi:10.1163/156854298X00183)

Herrel, A., Adriaens, D., Verraes, W. & Aerts, P. 2002 Bite performance in clariid fishes with hypertrophied jaw adductors as deduced by bite modeling. *J. Morphol.* **253**, 196–205. (doi:10.1002/jmor.1121)

Herrel, A., De Smet, A., Aguirre, L. F. & Aerts, P. 2008 Morphological and mechanical determinants of bite force in bats: do muscles matter? *J. Exp. Biol.* **211**, 86–91. (doi:10.1242/jeb.012211)

Herzog, W. 1994 Muscle. In *Biomechanics of the musculoskeltal system* (eds B. M. Nigg & W. Herzog), pp. 154–187. Chichester, UK: Wiley.

Huber, D. R. & Motta, P. J. 2004 Comparative analysis of methods for determining bite force in the spiny dogfish *Squalus acanthias*. *J. Exp. Zool.* **301A**, 26–37. (doi:10.1002/jez.a.20003)

Huber, D. R., Eason, T. G., Hueter, R. E. & Motta, P. J. 2005 Analysis of the bite force and mechanical design of the feeding mechanism of the durophagous horn shark *Heterodontus francisci*. *J. Exp. Biol.* **208**, 3553–3571. (doi:10.1242/jeb.01816)

Iordanski, N. N. 1990 Evolution of cranial kinesis in lower tetrapods. *Neth. J. Zool.* **40**, 32–54. (doi:10.1163/156854289X00174)

Iordanski, N. N. 1996 Evolution of the musculature of the jaw apparatus in the Amphibia. *Adv. Amph. Res. Former Sov. Union* **1**, 3–26.

Iordanski, N. N. 2000 Cranial kinesis in the amphibia: a review. *Zh. Obshch. Biol.* **61**, 102–118.

Kleinteich, T. & Haas, A. 2007 Cranial musculature in the larva of the caecilian, *Ichthyophis kohtaoensis* (Lissamphibia: Gymnophiona). *J. Morphol.* **268**, 74–88. (doi:10.1002/jmor.10503)

Kupfer, A. & Maraun, M. 2003 *Ichthyophis kohtaoensis* (Koh-Tao caecilian) diet. *Herpetol. Rev.* **34**, 226.

Kupfer, A., Nabhitabhata, J. & Himstedt, W. 2005 From water into soil: trophic ecology of a caecilian amphibian (genus *Ichthyophis*). *Acta. Oecol.* **28**, 95–105. (doi:10.1016/j.actao.2005.03.002)

Lawson, R. 1965 The anatomy of *Hypogeophis rostratus* Cuvier (Amphibia: Apoda or Gymnophiona). Part II. The musculature. *Proc. Univ. Newcastle Phil. Soc.* **1**, 52–63.

Luther, A. 1914 *N. trigeminus* versorgte Muskulatur der Amphibien. *Acta Soc. Sci. Fenn.* **7**, 3–151.

Marcus, H., Winsauer, O. & Hueber, A. 1933 Der kinetische Schädel von *Hypogeophis* und die Gehörknöchelchen. Beitrag zur Kenntnis der Gymnophionen XVIII. *Z. Anat. Entwicklungsgesch.* **100**, 149–193. (doi:10.1007/BF02118905)

Measey, G. J. & Herrel, A. 2006 Rotational feeding in caecilians: putting a spin on the evolution of cranial design. *Biol. Lett.* **2**, 485–487. (doi:10.1098/rsbl.2006.0516)

Measey, G. J., Gower, D. J., Oommen, O. V. & Wilkinson, M. 2004 A subterranean generalist predator: diet of the soil dwelling caecilian *Gegeneophis ramaswamii* (Amphibia; Gymnophiona; Caeciliidae) in southern India. *C. R. Biol.* **327**, 65–76. (doi:10.1016/j.crvi.2003.11.001)

Meryman, H. T. 1960 The preparation of biological museum specimens by freeze-drying. *Curator* **3**, 5–19.

Meryman, H. T. 1961 The preparation of biological museum specimens by freeze-drying: II. Instrumentation. *Curator* **4**, 153–174.

Meyers, J. J., Herrel, A. & Birch, J. 2002 Scaling of morphology, bite force and feeding kinematics in an iguanian and a scleroglossan lizard. In *Topics in functional and ecological vertebrate morphology* (eds P. Aerts, K. D'Août, A. Herrel & R. Van Damme), pp. 47–62. Maastricht, The Netherlands: Shaker Publishing.

Moodie, G. E. E. 1978 Observations on the life history of the caecilian *Typhlonectes compressicaudus* (Dumeril and Bibron) in the Amazon basin. *Can. J. Zool.* **56**, 1005–1008.

Nussbaum, R. A. 1983 The evolution of an unique dual jaw-closing mechanism in caecilians (Amphibia: Gymnophiona) and its bearing on caecilian ancestry. *J. Zool. Lond.* **199**, 545–554.

O'Reilly, J. C. 2000 Feeding in caecilians. In *Feeding: form, function and evolution in tetrapod vertebrates* (ed. K. Schwenk), pp. 149–166. San Diego, CA: Academic Press.

Presswell, B., Gower, D. J., Oommen, O. V., Measey, G. J. & Wilkinson, M. 2002 Scolecophidian snakes in the diets of south Asian caecilian amphibians. *Herpetol. J.* **12**, 123–126.

Radinsky, L. B. 1982 Evolution of skull shape in carnivores. 3. The origin and early radiation of the modern carnivore families. *Paleobiology* **8**, 177–195.

Riley, M. A. 1985 An analysis of masticatory form and function in three mustelids (*Martes americana*, *Lutra canadensis*, *Enhydra lutris*). *J. Mammal.* **66**, 519–528. (doi:10.2307/1380927)

Roelants, K., Gower, D. J., Wilkinson, M., Loader, S. P., Biju, S. D., Guillaume, K., Moriau, L. & Bossuyt, F. 2007 Global patterns of diversification in the history of modern amphibians. *Proc. Natl Acad. Sci. USA* **104**, 887–892. (doi:10.1073/pnas.0608378104)

Scapino, R. P. 1976 Function of the digastric muscle in carnivores. *J. Morphol.* **150**, 843–860. (doi:10.1002/jmor.1051500405)

Scapino, R. P. 1981 Morphological investigation into functions of the jaw symphysis in carnivorans. *J. Morphol.* **167**, 339–375. (doi:10.1002/jmor.1051670308)

Summers, A. P. & Wake, M. H. 2005 The retroarticular process, streptostyly and the caecilian jaw closing system. *Zoology* **108**, 307–315. (doi:10.1016/j.zool.2005.09.007)

Verdade, V. K., Schiesari, L. C. & Bertoluci, J. A. 2000 Diet of juvenile aquatic caecilians, *Typhlonectes compressicauda*. *J. Herpetol.* **34**, 291–293. (doi:10.2307/1565428)

Wake, M. H. 2003 The osteology of caecilians. In *Amphibian biology 5: osteology* (eds H. Heatwole & M. Davies), pp. 1810–1876. Chipping Norton, UK: Surrey Beatty and Sons.

Wake, M. H. & Hanken, J. 1982 Development of the skull of *Dermophis mexicanus* (Amphibia: Gymnophiona), with comments on skull kinesis and amphibian relationships. *J. Morphol.* **173**, 203–223. (doi:10.1002/jmor.1051730208)

Westneat, M. W. 2003 A biomechanical model for analysis of muscle force, power output and lower jaw motion in fishes. *J. Theor. Biol.* **223**, 269–281. (doi:10.1016/S0022-5193(03)00058-4)

Wiedersheim, R. 1879 *Die Anatomie der Gymnophionen*, p. 101. Jena, Germany: Fischer.

Wilkinson, M. & Nussbaum, R. A. 1997 Comparative morphology and evolution of the lungless caecilian *Atretochoana eiselti* (Taylor)(Amphibia: Gymnophiona: Typhlonectidae). *Biol. J. Linn. Soc. Lond.* **62**, 39–109.